Microscopic Simulation of Solid State Sintering Regarding Irregularly Shaped Powder Particles

Max Weiner

December 7, 2023

Contents

Preface **4**

Abbreviations **5**

1 Introduction **6**
1.1 The RefraBund Project 6
1.1.1 Aim and Scope 6
1.1.2 Project Structure 6
1.1.3 Process Routes 6
1.2 State of the Art 6
1.2.1 Basic Theory of Sintering 6
1.2.2 Sintering Models with Sharp Interfaces 6
1.2.3 Sintering Models with Diffuse Interfaces 6
1.2.4 Monte-Carlo-Methods (MCM) 6
1.2.5 The Thermodynamic Extremal Principle 6
1.2.6 Miscellaneous 8

2 Aim and Scope **9**

3 Powder Analysis and Representation **10**
3.1 Classic Methods of Powder Characterization 10
3.2 Particle Description by Parametrized Shape Functions 10
3.3 Characterization of Powders and Powder Mixtures 10

4 Model Development **11**
4.1 A Discrete Model of Powder Particles 11
4.2 Considerations on Free Surfaces 13
4.3 Considerations on Grain Boundaries 19
4.4 Considerations on Sinter Necks 21
4.5 Considerations on Grain-Matrix Interfaces 21
4.6 Application of the Thermodynamic Extremal Principle 21
4.6.1 Time Scale Definition 22
4.6.2 Choice of Variables 22
4.6.3 Dissipation $\mathcal{D}$ 22
4.6.4 Dissipation Function $\mathcal{Q}$ 23
4.6.5 Required Constraints $\boldsymbol{f}$ 23
4.6.6 Additonal Constraints $\boldsymbol{g}$ 23

5 Software Implementation of the Model **24**
5.1 Representation of Particles and Nodes 24
5.2 Numerical Solution Procedure 24
5.3 Calculation and Extraction of Key Features 24

6 Model Validation **25**
6.1 Investigations on Simple Test Cases 25
6.1.1 A Single Particle Free in Space 25
6.1.2 A Particle Pair Free in Space 25
6.1.3 A Particle Pair at Different Contact Angles 25
6.1.4 A Particle Pair with Asymmetric Material Properties 25
6.1.5 A Single Particle Embedded in a Matrix 25
6.1.6 A Particle Pair Embedded in a Matrix 25
6.2 Experimental Validation Counter Bulk Sintering Trials 25

7 Summary and Outlook **26**

List of Figures **27**

List of Tables **28**

Bibliography **29**

Preface

Abbreviations

BFGS breadth-first graph search 12

DAG directed acyclic graph 12

DFGS depth-first graph search 13

RCE ring-closing edge 12

TEP thermodynamic extremal principle 6

1 Introduction

1.1 The RefraBund Project

1.1.1 Aim and Scope

1.1.2 Project Structure

1.1.3 Process Routes

1.2 State of the Art

1.2.1 Basic Theory of Sintering

1.2.2 Sintering Models with Sharp Interfaces

1.2.3 Sintering Models with Diffuse Interfaces

1.2.4 Monte-Carlo-Methods (MCM)

Classic Monte Carlo Methods

Kinetic Monte Carlo Methods

1.2.5 The Thermodynamic Extremal Principle

General things about internal state and non-equilibrium
Applications

Classic Formulation

The classic formulation of the thermodynamic extremal principle (TEP) was basically formulated by Svoboda and Turek [4], however dependent on the works of Ziegler [5, 6] and Onsager [3]. It is based on the assumption, that the dissipation in the system is always maximized with respect to thermodynamic and kinetic constraints. This is equivalent to the statement, that the system always tries to approach the equilibrium as fast as possible.

The dissipation $\mathcal{D}$ can be formulated as in Equation 1.1a in dependence on the vector of external state variables $\boldsymbol{X}$, the vector of internal state variables $\boldsymbol{x}$ and the velocity vector of internal state variables $\dot{\boldsymbol{x}}$. It is a bilinear form in the velocity vector of internal state variables and the vector of thermodynamik forces. The latter can be expressed as $\partial G(\boldsymbol{X}, \boldsymbol{x})/\partial \boldsymbol{x}$, where G is the Gibbs energy of the system. The Gibbs energy is as state function independent of $\dot{\boldsymbol{x}}$, thus the thermodynamic forces do not include any kinetic constraints. Since $\mathcal{D}$ is linear in $\dot{\boldsymbol{x}}$, maximizing without further constraints is not meaningful. Therefore, an additional dissipation function $\mathcal{Q}$ is introduced, which must be always equal to $\mathcal{D}$, since both describe the dissipation of the process (compare Equation 1.1b). However, $\mathcal{Q}$ is formulated in terms of the kinetic conditions of the process and is generally and non-linear form in $\dot{\boldsymbol{x}}$, often a quadratic form. The actual form

of $\mathcal{Q}$ heavily depends on the regarded process, but it commonly includes empirical kinetic material parameters such as diffusion coefficients or mobilities.

$$\mathcal{D}(\boldsymbol{X}, \boldsymbol{x}, \dot{\boldsymbol{x}}) = \frac{\partial G(\boldsymbol{X}, \boldsymbol{x})}{\partial \boldsymbol{x}} \cdot \dot{\boldsymbol{x}} \rightarrow \max_{\dot{\boldsymbol{x}}} \tag{1.1a}$$

$$\mathcal{D}(\boldsymbol{X}, \boldsymbol{x}, \dot{\boldsymbol{x}}) - \mathcal{Q}(\boldsymbol{X}, \boldsymbol{x}, \dot{\boldsymbol{x}}) = 0 \tag{1.1b}$$

The constrained optimization problem in Equation 1.1 can be solved using the Lagrange formalism. The problem is reformulated as the Lagrange functional $\mathcal{L}$ in Equation 1.2 with the additional parameter λ.

$$\mathcal{L} = \mathcal{D}(\boldsymbol{X}, \boldsymbol{x}, \dot{\boldsymbol{x}}) + \lambda \left(\mathcal{D}(\boldsymbol{X}, \boldsymbol{x}, \dot{\boldsymbol{x}}) - \mathcal{Q}(\boldsymbol{X}, \boldsymbol{x}, \dot{\boldsymbol{x}}) \right) \tag{1.2}$$

Setting the gradient of $\mathcal{L}$ with respect to $\dot{\boldsymbol{x}}$ and λ equal zero gives the optimum of the dissipation $\mathcal{D}$ under the given constraints. Note that the derivative with respect to λ is always identical to the constraint equation.

$$\mathcal{L}_{\dot{\boldsymbol{x}}} = (1 + \lambda) \frac{\partial G(\boldsymbol{X}, \boldsymbol{x})}{\partial \boldsymbol{x}} - \lambda \frac{\partial \mathcal{Q}(\boldsymbol{X}, \boldsymbol{x}, \dot{\boldsymbol{x}})}{\partial \dot{\boldsymbol{x}}} \stackrel{!}{=} 0 \tag{1.3a}$$

$$\mathcal{L}_{\lambda} = \mathcal{D}(\boldsymbol{X}, \boldsymbol{x}, \dot{\boldsymbol{x}}) - \mathcal{Q}(\boldsymbol{X}, \boldsymbol{x}, \dot{\boldsymbol{x}}) \stackrel{!}{=} 0 \tag{1.3b}$$

For the simple case of $\mathcal{Q}$ being quadratic in $\dot{\boldsymbol{x}}$ the solution of the system is given in Equation 1.4, which is a linear system of equations of the same size as $\dot{\boldsymbol{x}}$. Compare Svoboda and Turek [4] and Fischer, Svoboda, and Petryk [1] on this.

$$-\frac{\partial G(\boldsymbol{X}, \boldsymbol{x})}{\partial \boldsymbol{x}} = \frac{1}{2} \frac{\partial \mathcal{Q}(\boldsymbol{X}, \boldsymbol{x}, \dot{\boldsymbol{x}})}{\partial \dot{\boldsymbol{x}}} \tag{1.4}$$

Note, that for this formulation it is required, that the dissipation $\mathcal{D}$ and the dissipation function $\mathcal{Q}$ must depend on the same kinetic variables $\dot{\boldsymbol{x}}$. Often the fluxes $\boldsymbol{j}$ are used therein.

Generalized Formulation

Recently, Hackl, Fischer, and Svoboda [2] published a generalized formulation of the principle breaking up the need to have the same kinetic variables in the dissipation $\mathcal{D}$ and the dissipation function $\mathcal{Q}$. The following elaborations use a different notation than in the reference, which fits better to the needs of the application in section 4.6, but the meaning is generally equivalent. The dissipation $\mathcal{D}$ is defined in the same way as before, but the dissipation function $\mathcal{Q}$ does not include the velocities of internal state $\dot{\boldsymbol{x}}$, but instead the fluxes $\boldsymbol{j}$ as in Equation 1.5b. Note, that the velocities $\dot{\boldsymbol{x}}$ are *not* required to be identical to the fluxes $\boldsymbol{j}$ here, neither they must have the same size. The connections between the velocities $\dot{\boldsymbol{x}}$ and the fluxes $\boldsymbol{j}$ are introduced by the constraints $\boldsymbol{f}$ as in Equation 1.5c. These are required to be able to solve the problem, so they shall be called *required* constraints hereinafter. $\boldsymbol{f}$ and $\boldsymbol{j}$ must be of same size. But it is also possible to include several *additional* constraints $\boldsymbol{g}$. These may be used for other requirements on the validity of the model, for example geometric constraints. The constraints may include several *auxiliary variables* $\boldsymbol{\xi}$ that are not part of $\boldsymbol{x}$ or $\boldsymbol{j}$ and occur therefore neither in $\mathcal{D}$ nor $\mathcal{Q}$. See section 4.6 for details on their application.

$$\mathcal{D}(\boldsymbol{X}, \boldsymbol{x}, \dot{\boldsymbol{x}}) = \frac{\partial G(\boldsymbol{X}, \boldsymbol{x})}{\partial \boldsymbol{x}} \cdot \dot{\boldsymbol{x}} \rightarrow \max_{\dot{\boldsymbol{x}}} \tag{1.5a}$$

$$\mathcal{D}(\boldsymbol{X}, \boldsymbol{x}, \dot{\boldsymbol{x}}) - \mathcal{Q}(\boldsymbol{X}, \boldsymbol{x}, \boldsymbol{j}) = 0 \tag{1.5b}$$

$$\boldsymbol{f}(\boldsymbol{X}, \boldsymbol{x}, \dot{\boldsymbol{x}}, \boldsymbol{j}, \boldsymbol{\xi}) = 0 \tag{1.5c}$$

$$\boldsymbol{g}(\boldsymbol{X}, \boldsymbol{x}, \dot{\boldsymbol{x}}, \boldsymbol{j}, \boldsymbol{\xi}) = 0 \tag{1.5d}$$

With this generalized formulation the Lagrange functional writes as in Equation 1.6. Here we have more Lagrange parameters. λ_1 is equivalent to the classic formulation. The vector parameters $\boldsymbol{\lambda_2}$ and $\boldsymbol{\lambda_3}$ for the required and additional constraints are of the same size as $\boldsymbol{f}$ resp. $\boldsymbol{g}$.

$$\mathcal{L} = \mathcal{D}(\boldsymbol{X}, \boldsymbol{x}, \dot{\boldsymbol{x}}) + (\mathcal{D}(\boldsymbol{X}, \boldsymbol{x}, \dot{\boldsymbol{x}}) - \mathcal{Q}(\boldsymbol{X}, \boldsymbol{x}, \boldsymbol{j}))\, \lambda_1 + \boldsymbol{f}^{\mathrm{T}}(\boldsymbol{X}, \boldsymbol{x}, \dot{\boldsymbol{x}}, \boldsymbol{j}, \boldsymbol{\xi}) \cdot \boldsymbol{\lambda_2} + \boldsymbol{g}^{\mathrm{T}}(\boldsymbol{X}, \boldsymbol{x}, \dot{\boldsymbol{x}}, \boldsymbol{j}, \boldsymbol{\xi}) \cdot \boldsymbol{\lambda_3} \tag{1.6}$$

As before, the gradient of $\mathcal{L}$ is set equal to zero to obtain the constrained optimum. Finding a simplified equation system as done above (Equation 1.4) is here not possible due to the constraints.

$$\mathcal{L}_{\dot{\boldsymbol{x}}} = \frac{\partial G(\boldsymbol{X}, \boldsymbol{x})}{\partial \boldsymbol{x}} (1 + \lambda_1) + \frac{\partial \boldsymbol{f}^{\mathrm{T}}(\boldsymbol{X}, \boldsymbol{x}, \dot{\boldsymbol{x}}, \boldsymbol{j}, \boldsymbol{\xi})}{\partial \dot{\boldsymbol{x}}} \cdot \boldsymbol{\lambda_2} + \frac{\partial \boldsymbol{g}^{\mathrm{T}}(\boldsymbol{X}, \boldsymbol{x}, \dot{\boldsymbol{x}}, \boldsymbol{j}, \boldsymbol{\xi})}{\partial \dot{\boldsymbol{x}}} \cdot \boldsymbol{\lambda_3} \stackrel{!}{=} 0 \tag{1.7a}$$

$$\mathcal{L}_{\boldsymbol{j}} = -\frac{\partial \mathcal{Q}(\boldsymbol{X}, \boldsymbol{x}, \boldsymbol{j})}{\partial \boldsymbol{j}} \lambda_1 + \frac{\partial \boldsymbol{f}^{\mathrm{T}}(\boldsymbol{X}, \boldsymbol{x}, \dot{\boldsymbol{x}}, \boldsymbol{j}, \boldsymbol{\xi})}{\partial \boldsymbol{j}} \cdot \boldsymbol{\lambda_2} + \frac{\partial \boldsymbol{g}^{\mathrm{T}}(\boldsymbol{X}, \boldsymbol{x}, \dot{\boldsymbol{x}}, \boldsymbol{j}, \boldsymbol{\xi})}{\partial \boldsymbol{j}} \cdot \boldsymbol{\lambda_3} \stackrel{!}{=} 0 \tag{1.7b}$$

$$\mathcal{L}_{\boldsymbol{\xi}} = \frac{\partial \boldsymbol{f}^{\mathrm{T}}(\boldsymbol{X}, \boldsymbol{x}, \dot{\boldsymbol{x}}, \boldsymbol{j}, \boldsymbol{\xi})}{\partial \boldsymbol{\xi}} \cdot \boldsymbol{\lambda_2} + \frac{\partial \boldsymbol{g}^{\mathrm{T}}(\boldsymbol{X}, \boldsymbol{x}, \dot{\boldsymbol{x}}, \boldsymbol{j}, \boldsymbol{\xi})}{\partial \boldsymbol{\xi}} \cdot \boldsymbol{\lambda_3} \stackrel{!}{=} 0 \tag{1.7c}$$

$$\mathcal{L}_{\lambda_1} = \mathcal{D}(\boldsymbol{X}, \boldsymbol{x}, \dot{\boldsymbol{x}}) - \mathcal{Q}(\boldsymbol{X}, \boldsymbol{x}, \boldsymbol{j}) \stackrel{!}{=} 0 \tag{1.7d}$$

$$\mathcal{L}_{\boldsymbol{\lambda}_2} = \boldsymbol{f}(\boldsymbol{X}, \boldsymbol{x}, \dot{\boldsymbol{x}}, \boldsymbol{j}, \boldsymbol{\xi}) \stackrel{!}{=} 0 \tag{1.7e}$$

$$\mathcal{L}_{\boldsymbol{\lambda}_3} = \boldsymbol{g}(\boldsymbol{X}, \boldsymbol{x}, \dot{\boldsymbol{x}}, \boldsymbol{j}, \boldsymbol{\xi}) \stackrel{!}{=} 0 \tag{1.7f}$$

1.2.6 Miscellaneous

2 Aim and Scope

This work is intended to create and evaluate a novel model approach for sintering of irregularly shaped particles. The model is based on a *finite differences* (FD) approach of particle description, thus the interfaces are described as sharp lines. FOr the solution of the complicated partial differential equation system describing the diffusional flows and geometry evolution, the *thermodynamic extremal principle* (TEP) shall be applied. The model shall be restricted to 2D-space as a proof of concept, but may be extended to 3D-space as well. The latter is out of scope of this work.

The work resides under the circumstances of the RefraBund project as described in section 1.1. Therefore, the following influences shall be included in the model and investigated by simulation as well experiment.

Multi-Material Powder The investigated material consists of aluminium oxide powder as well as metallic niobium resp. tantalum powder. The model must therefore be able to respect different material properties on particles in contact to each other with their implication of grain boundary shape and kinetic behavior.

Multi-Scale Powder For achieving good thermal shock properties a component shall consist of coarse-grained material with fine-grained additions as filler and bonder. The model must be able to deal with particle sizes that differ by several orders of magnitude, which is mainly a topic of computational effort and numerical stability.

Aggregate Powders The coarse grained powder is obtained be sintering of fine-grained composite powders to produce aggregate particles. The aggregate particles are not homogeneous in their properties and include a certain porosity. The model must include contacts of aggregate particles by average approaches to circumvent the need of local structure description and modelling.

Powder Mixture The production process involves mixing of different powder fractions to obtain optimal properties in processing and application. The mixing shall be modelled by statistical approaches to enable the investigation of different powder mixture to support product development.

The predictions of the model are characterized in this work in comparison to other models. The model is validated against sintering experiments under consideration of microstructure and physical material properties.

3 Powder Analysis and Representation

3.1 Classic Methods of Powder Characterization

3.2 Particle Description by Parametrized Shape Functions

3.3 Characterization of Powders and Powder Mixtures

4 Model Development

4.1 A Discrete Model of Powder Particles

- Particles, Coordinate System
- Node Types
- Multi-Scale Considerations, Matrix

Continuous description of the particle surface geometry is only possible for nearly ideal geometries. For complicated geometries a discretized approach is feasible. For the current work, the concept of a node shall be introduced. A node is here considered as a discrete point of the particle surface connected with its neighbors by straight lines. The spline of those lines is defining the surface of the particle.

The location of each node in space is defined by a tuple of polar coordinates (φ, r), where φ is the angle coordinate and r the radius resp. distance from origin. The origin of the polar coordinates is distinct for each particle and is considered as the center of the particle, although it is generally not identical with the barycenter of the particle. But the center of the particle is used as an anchor for defining a particles postions in space. With this concept the particle can be moved in space without translating the surface node coordinates and the description of node evolution is simplified, since only the local geometry must be regarded. Particle movement occurs due to diffusional fluxes in the grain boundaries, which is macroscopically observed as shrinkage. The location of a particle is defined by the cartesian coordinates of its center x and y, as well as a rotation angle ω with the center as pole. The rotation angle always counts from the x-axis on in mathematical direction. The rotation angle also defines the origin axis of the particles local coordinate system. See Figure 4.1 for illustration on this.

In regard of sintering processes, the contact properties of multiple particles are investigated. The common interface of two particles in contact is commonly called a sinter neck. It consists of a grain boundary bounded by triple points of the grain boundary and the two adjacent free surfaces. Figure 4.2 shows such a contact of two particles. Until here, three types of nodes can be identified:

Surface Nodes forming the free surface of a particle in contact to atmosphere or vacuum (black).

Grain Boundary Nodes forming the grain boundary in a particle contact (dark blue).

Neck Nodes representing the triple point between grain boundary and two surfaces (dark red).

Details on the conditions at those nodes are given in the following sections. The particles are named as *parent* and *child*, since every particle contact shall be regarded in a hierarchical manner. The reason for that lies in the graph description of contact topology described below. The contact is characterized by the length and the direction of the line connecting the involved particles' centers. Since every particle has its own polar coordinate system, measures of contact and coordinates of nodes involved can be regarded in either the parent's or the child's coordinate system.

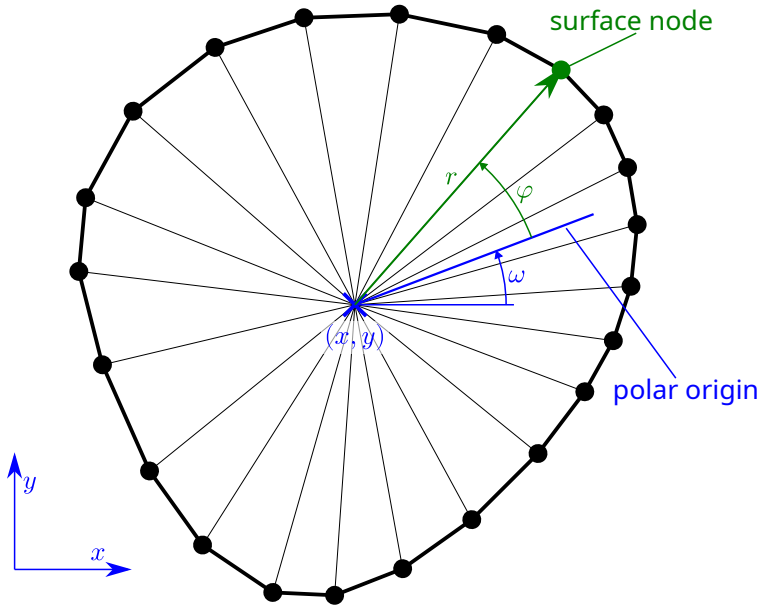

Figure 4.1: Position of a Particle and Its Local Coordinate System

The coordinate system used shall be denoted hereinafter by $^{|\square}$ superscripts where necessary as done in the figure. So the direction ange of the contact is $\varphi_{\mathrm{C}}^{|\mathrm{p}}$ or $\varphi_{\mathrm{C}}^{|\mathrm{c}}$ in means of the parent's or the child's coordinate system, respectively. The coordinates of one neck node are shown in the figure as $(\varphi^{|\mathrm{p}}, r^{|\mathrm{p}})$ and $(\varphi^{|\mathrm{c}}, r^{|\mathrm{c}})$. Note, that both tuples represent the same point in space.

The contact topology of multiple particles can be described as a graph, where the vertices correspond to particles and the edges correspond to contact relations between the particles. The undirected graph structure of a particle contact is shown in Figure 4.3. The indices of the vertices are at this point arbitrary, but are reused in the same way in the following.

For simulation purposes, the introduction of a hierarchy in the particle contacts is feasible to introduce a specific order for equation construction. More specifically the particle contacts shall be described as a directed acyclic graph (DAG). Such a graph can always be constructed from a given undirected graph by performing a breadth-first graph search (BFGS) starting at the desired root vertex and dropping all edges pointing back to the parent. An example of such a structure in shown in Figure 4.4. The particle labeled with index 0 is the *root* of the graph, the only vertex that has no incoming edges. In general, the root of the particle graph can be chosen arbitrarily, but for efficiency reasons, it should be a particle which leads to a graph as flat as possible. The root particle has a fixed position in space and therefore acts as origin for all coordinate systems used throughout the calculations. There may be cases, where the particle graph has rooted tree structure, which simplifies the problem significantly, since then all particles are able to move freely. Edges like the red one in the figure break the tree structure. Note, that they do not form cycles in the DAG in the meaning of graph theory, since the edges are directed. But in terms of the underlying undirected graph they are anyway cycles. To avoid ambiguities, the term ring contact shall be used here instead. Ring contacts introduce additional constraints to the particle movement, since each particle in the ring influences the movement of the others. The edges closing a ring are named correspondingly as ring-closing edges (RCEs).

RCEs are discovered during a BFGS when a vertex is encountered that was already marked as visited. To be able to construct geometric constraints on particle movement, a ring path must be defined. A ring path is a path following the cycle in the undirected graph, the currently regarded

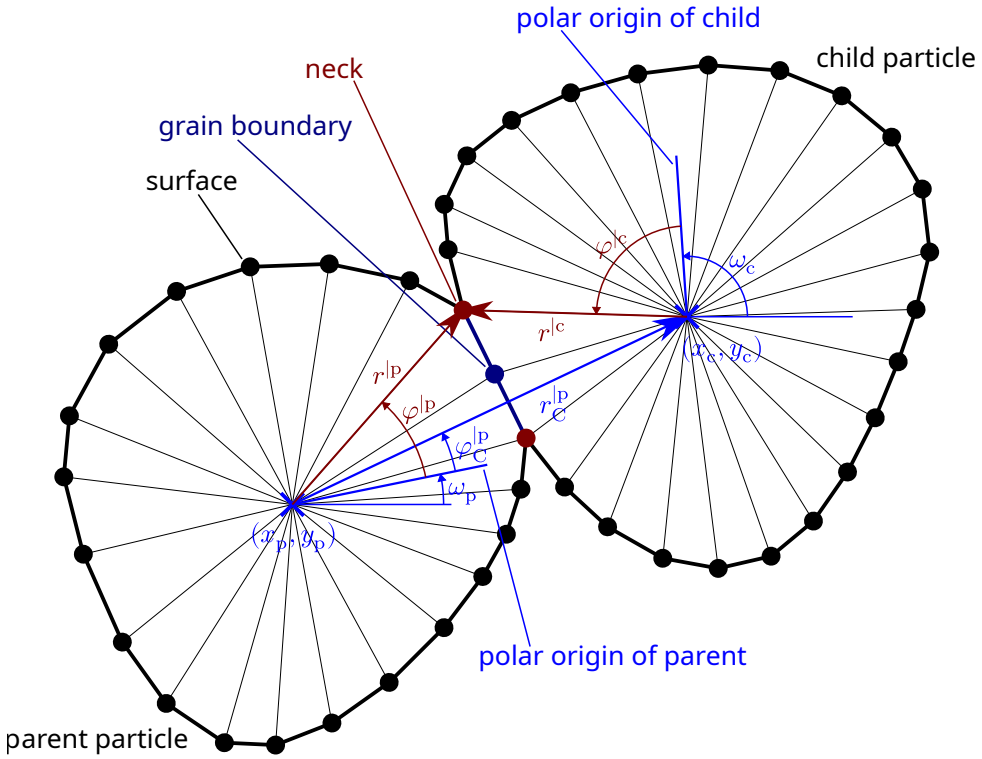

Figure 4.2: Contact of Two Particles with Respective Properties

ring corresponds to. It is generally not unique, but this is also not necessary. To find a ring path, a depth-first graph search (DFGS) is performed on the undirected particle graph with the ring closing edge removed. The removed edge is afterwards appended to the path to close the ring. The procedure is illustrated in Figure 4.5.

4.2 Considerations on Free Surfaces

If a node is displaced (shifted) in space, a change in Gibbs energy occurs due to the change in surface resp. interface area. The amount of energy bound in a surface or interface is described by the interface energy γ. Since a 2D problem is regarded, the length of the surface line a is a measure of present surface area. The change of Gibbs energy due to node shifting is described by Equation 4.1 with the prime values as measures after shifting.

$$\delta G_\perp = \left(a'_\mathrm{u} - a_\mathrm{u} + a'_\mathrm{l} - a_\mathrm{l}\right)\gamma_\mathrm{S} \tag{4.1}$$

The shifting of nodes is separated into two components as shown in Figure 4.6. The normal vector points under an angle of $\delta_\perp$ acc. to Equation 4.2 to both surface lines.

$$\delta_\perp = \pi - \frac{1}{2}\left(\alpha_\mathrm{u} + \alpha_\mathrm{l}\right) \tag{4.2}$$

With a certain normal shift $\delta s_\perp$, the surface lengths after shifting are calculated by Equation 4.3 and Equation 4.4.

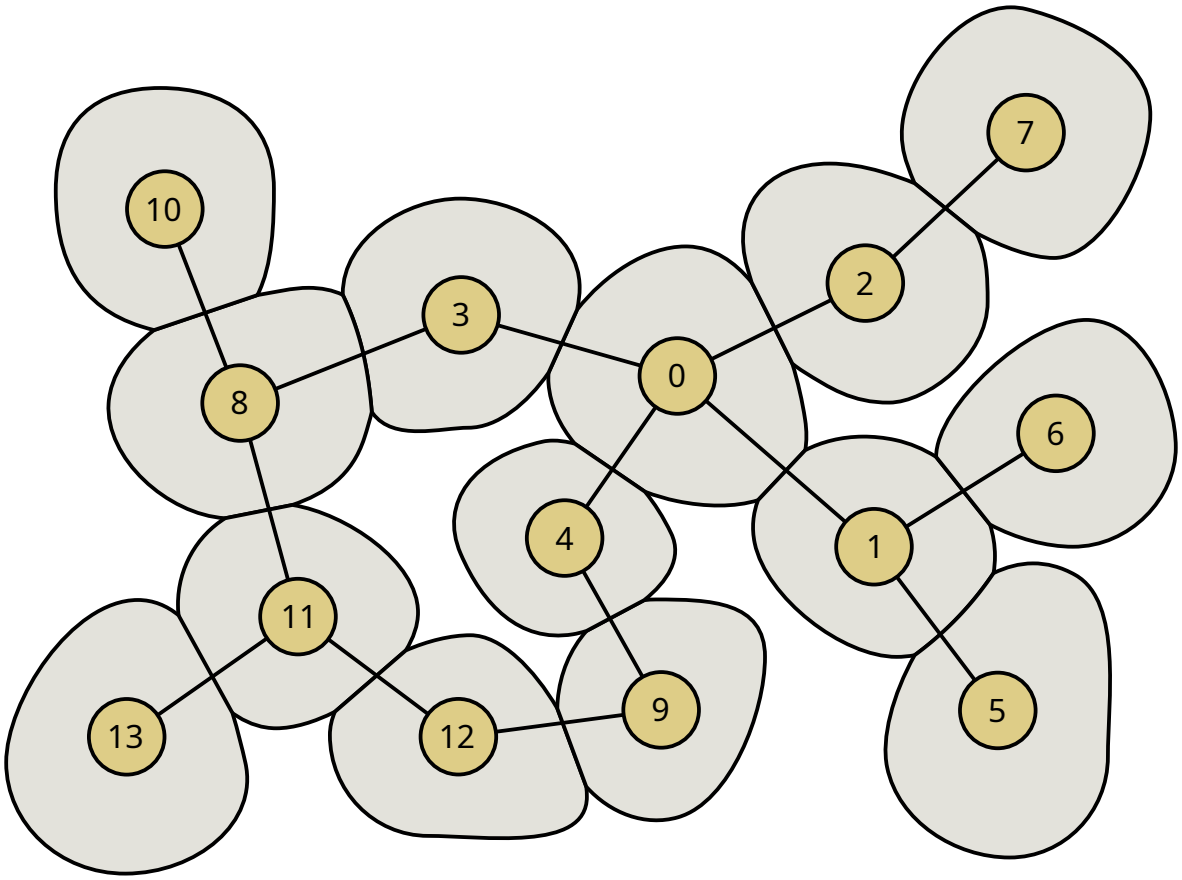

Figure 4.3: Undirected Particle Graph Representing Contact Conditions

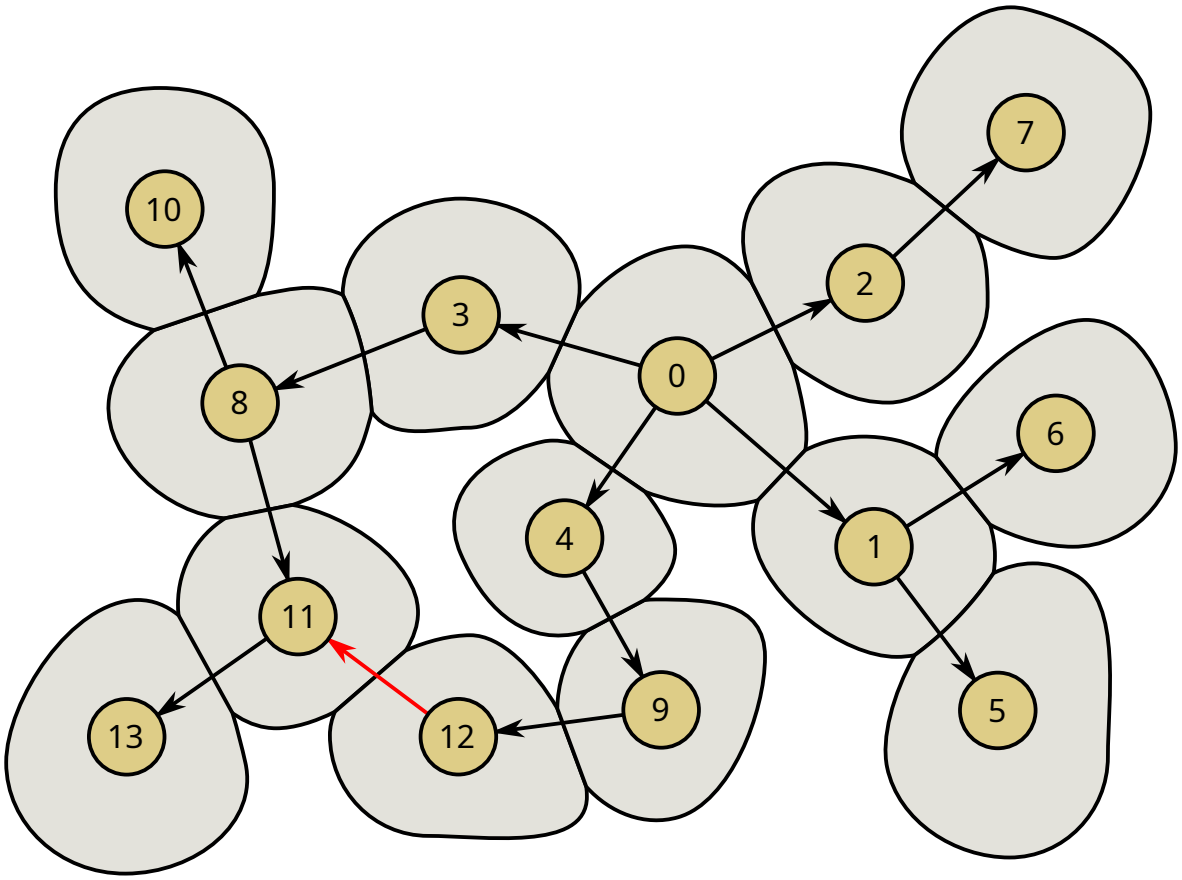

Figure 4.4: Directed Acyclic Graph Structure of Particle Contacts Rooted at Vertex 0

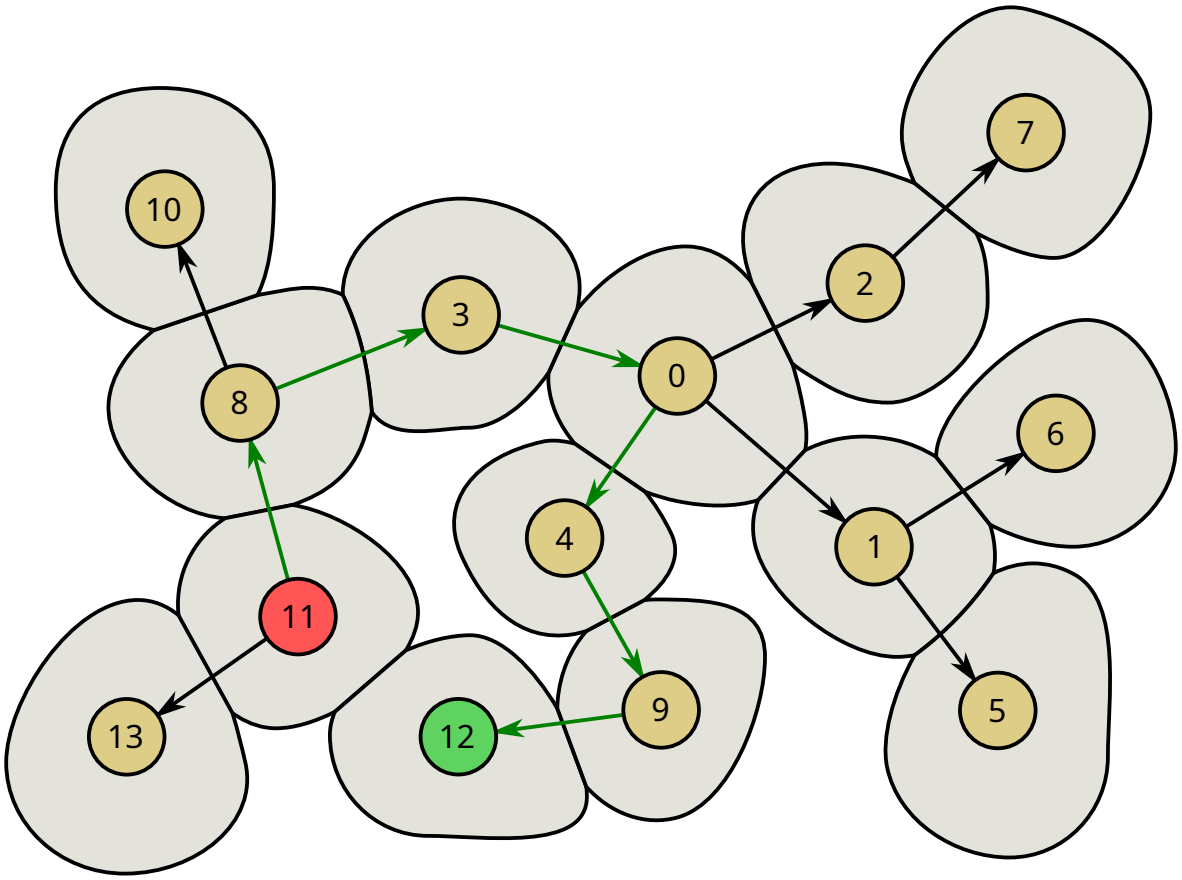

Figure 4.5: Ring Path Search Using a Depth-First Graph Search

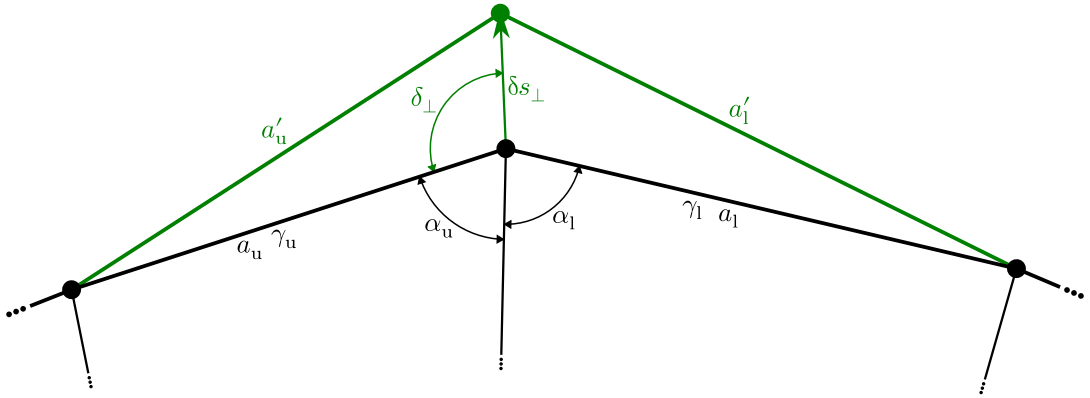

(a) Normal Direction

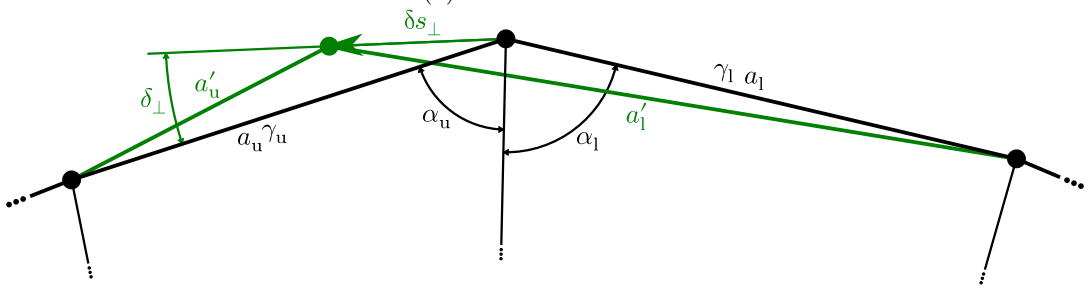

(b) Tangential Direction

Figure 4.6: Shifting of Surface Nodes

$$a'_\mathrm{u} = \sqrt{a_\mathrm{u}^2 + \delta s_\perp^2 - 2a_\mathrm{u}\delta s_\perp \cos\delta_\perp} \tag{4.3}$$

$$a'_\mathrm{l} = \sqrt{a_\mathrm{l}^2 + \delta s_\perp^2 - 2a_\mathrm{l}\delta s_\perp \cos\delta_\perp} \tag{4.4}$$

The slope of the tangent in $\delta s_\perp = 0$ is calculated as in Equation 4.5. Figure 4.7a shows the change in Gibbs energy due to normal shifting with different values of $\delta_\perp$ and γ. A $\delta_\perp > 90°$ means a convex surface, thus energy gain when inward shifting (negative $\delta s_\perp$). A $\delta_\perp < 90°$ means a concave surface, thus energy gain when outward shifting (positive $\delta s_\perp$). A $\delta_\perp = 90°$ means a even surface, thus energy loss in both shifting directions. Note, that the slope is dependent on the sum of γ_u and γ_l, whereas the monotonicity depends on $\delta_\perp$.

$$\frac{\partial G}{\partial s_\perp} = \lim_{\delta s_\perp \to 0} \frac{\delta G_\perp}{\delta s_\perp} = -\left(\gamma_\mathrm{u} + \gamma_\mathrm{l}\right)\cos\delta_\perp \tag{4.5}$$

$$\frac{\partial V}{\partial s_\perp} = \frac{1}{2}\left(a_\mathrm{u} + a_\mathrm{l}\right)\sin\delta_\perp \tag{4.6}$$

Regarding the normal shifting, the direction vector is under an angle of $\delta_\parallel$ acc. to. Equation 4.7 to the upper surface line.

$$\delta_\parallel = \delta_\perp - \frac{\pi}{2} \tag{4.7}$$

The change in Gibbs energy is calculated in a similar way acc. to Equation 4.8, but the shifted surface lengths calculate as in Equation 4.9 and Equation 4.10 in dependence on the tangential shift $\delta s_\parallel$. Note the signs before the cosine terms.

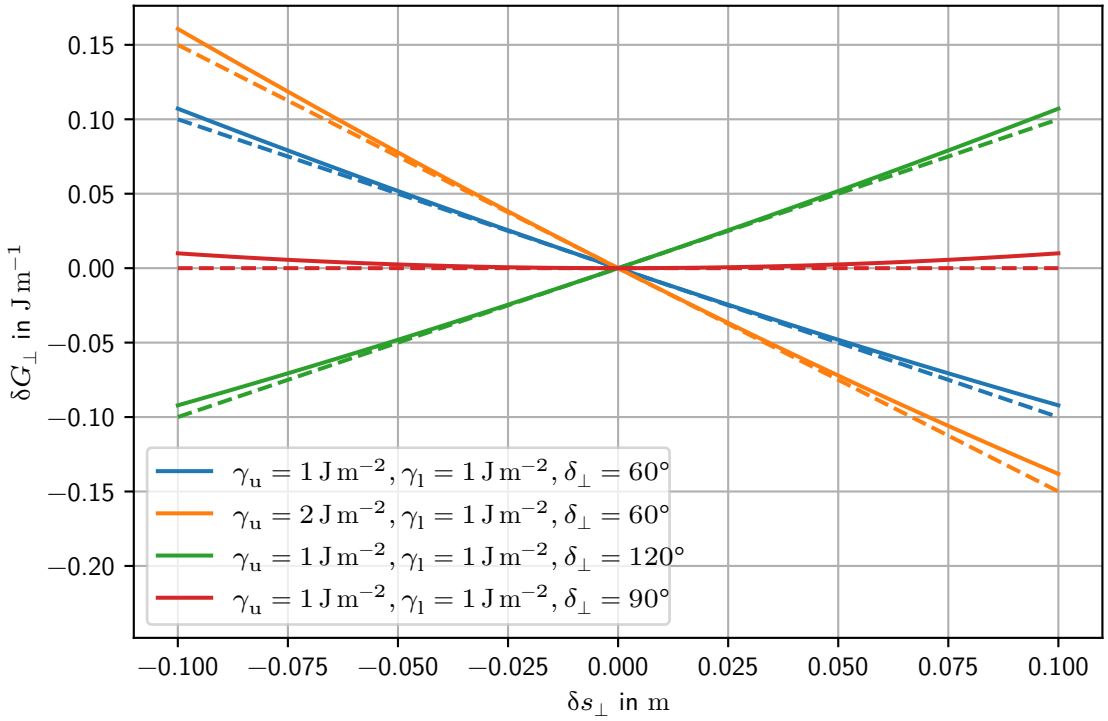

(a) Normal Direction

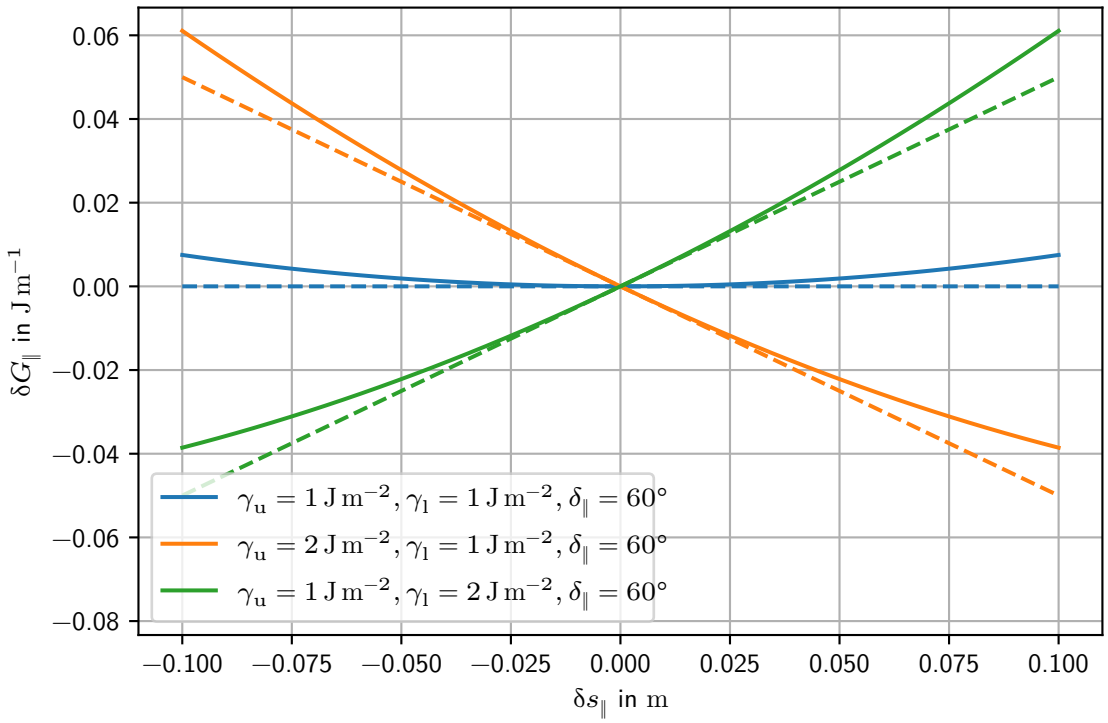

(b) Tangential Direction

Figure 4.7: Change in Gibbs Energy Due to Node Shifting (tangents dashed)

$$\delta G_{\perp} = (a'_{\mathrm{u}} - a_{\mathrm{u}} + a'_{\mathrm{l}} - a_{\mathrm{l}})\,\mathrm{S}\gamma \tag{4.8}$$

$$a'_{\mathrm{u}} = \sqrt{a_{\mathrm{u}}^2 + \delta s_{\parallel}^2 - 2a_{\mathrm{u}}\delta s_{\parallel}\cos\delta_{\parallel}} \tag{4.9}$$

$$a'_{\mathrm{l}} = \sqrt{a_{\mathrm{l}}^2 + \delta s_{\parallel}^2 + 2a_{\mathrm{l}}\delta s_{\parallel}\cos\delta_{\parallel}} \tag{4.10}$$

The slope of the tangent in $\delta s_{\parallel} = 0$ is calculated as in Equation 4.11. Figure 4.7b shows the change in Gibbs energy due to normal shifting with different values of γ. The slope and monotonicity of these curves is here dependent on the *difference* of γ_{u} and γ_{l}. The convexity or concavity of the surface is here only of minor importance. Whether the interface with higher γ is located on the upper or lower side determines the monotonicity of the curves. In the special case when $\gamma_{\mathrm{u}} = \gamma_{\mathrm{l}}$, the curve has a minimum in $\delta s_{\parallel} = 0$, meaning that any shift will produce an energy loss. This is the case on all nodes except neck nodes.

$$\frac{\partial G}{\partial s_{\parallel}} = \lim_{\delta s_{\parallel}\to 0}\frac{\delta G_{\parallel}}{\delta s_{\parallel}} = -\left(\gamma_{\mathrm{u}} - \gamma_{\mathrm{l}}\right)\cos\delta_{\parallel} \tag{4.11}$$

$$\frac{\partial V}{\partial s_{\parallel}} = \frac{1}{2}\left(a_{\mathrm{l}} - a_{\mathrm{u}}\right)\sin\delta_{\parallel} \tag{4.12}$$

4.3 Considerations on Grain Boundaries

In contrast to free surfaces, where the geometric evolution of a node is not constrained by the surrounding space, in grain boundaries the node shifting acts counter the solid material of the other particle. This introduces additional constraints, since the grain boundary must not form holes and must not overlap. The geometric constraints are dependent on the local evolution of the grain boundary nodes, as well as the relative position change of the particles.

Starting from a compact grain boundary, meaning that there are no holes and/or overlap present within it, the condition of maintaining the compactness of the grain boundary can be formulated as follows, if the postions of the particles are fixed.

$$\mathrm{L}\delta s_{\perp} = -\mathrm{R}\delta s_{\perp} \tag{4.13}$$

$$\mathrm{L}\delta s_{\parallel} = -\mathrm{R}\delta s_{\parallel} \tag{4.14}$$

But in reality the positions of particles to each other change, which can be observed macroscopically as shrinkage. However, the relation between node shifting and particle movement cannot be easily formulated, since the particle movement is effected by the ensemble of all nodes involved in the contact. But, we can formulate the influence of shifting one node in normal or tangential direction on the opposite particle, if that particle is assumed as invariant in shape. Each contact node has two sets of coordinates, one in the terms of the one particle, one in terms of the other. However, they represent both the same point in space.

Figure 4.8 and Figure 4.9 show the geometric conditions of such a shift. The left particle (index L) changes its shape by shifting a single regarded node, while the right particle (index R) is invariant. The particles are assumed to be solely connected in the regarded node, the influence of adjacent nodes is disregarded. Therefore, the radius line of the node regarded from the right

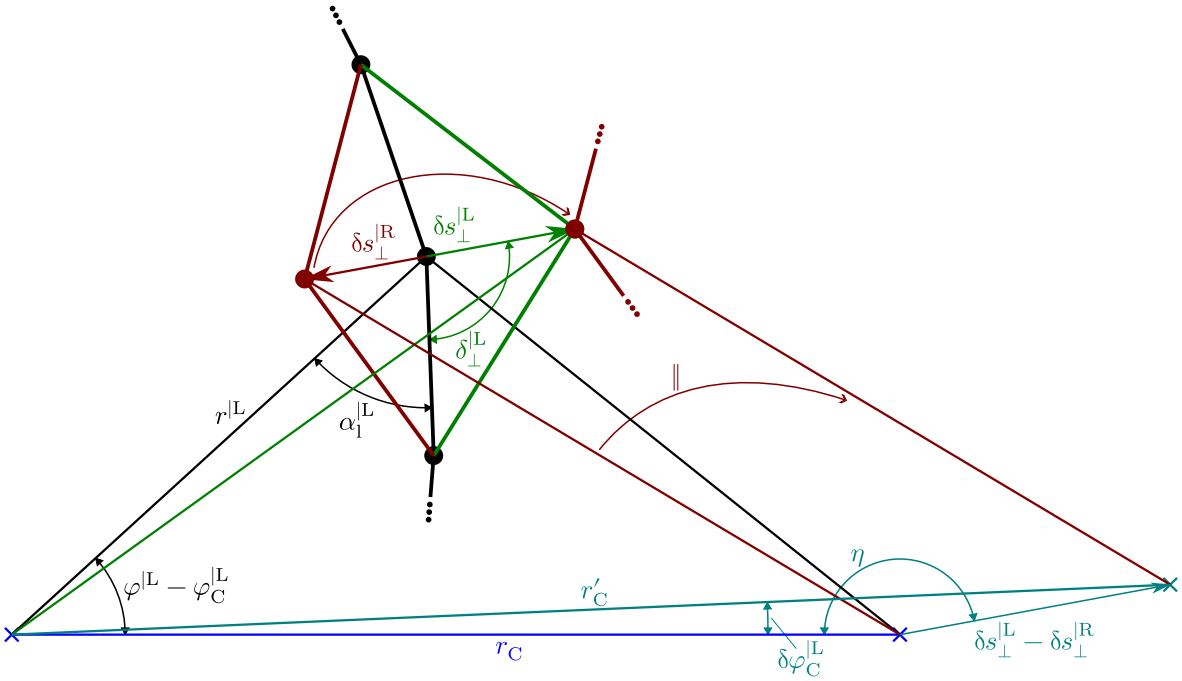

Figure 4.8: Effect of Normal Node Shifting on Particle Postion

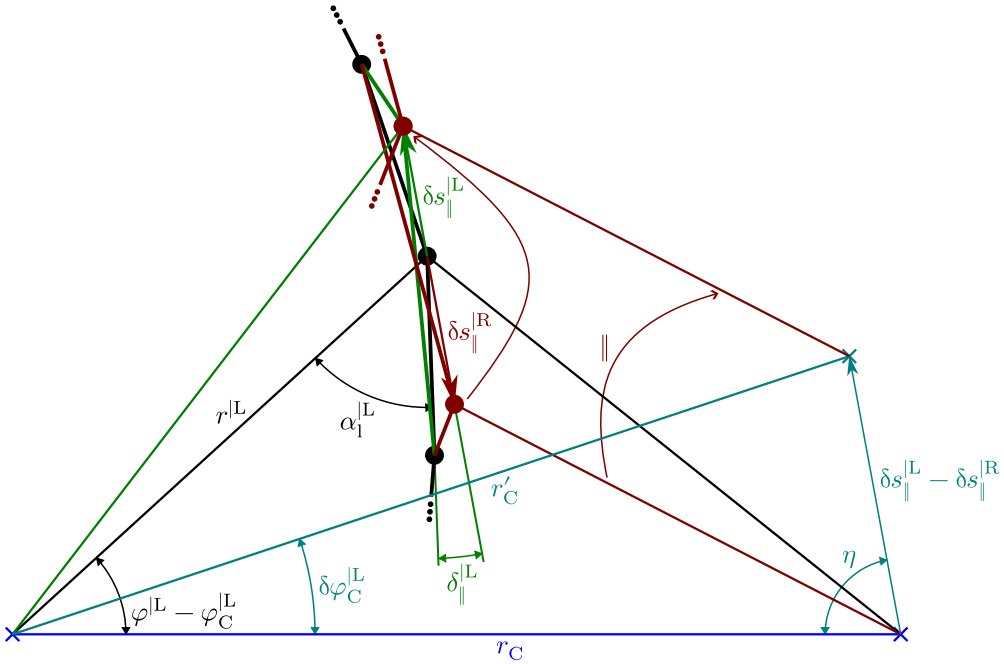

Figure 4.9: Effect of Tangential Node Shifting on Particle Postion

particle retains the same length and angle to the surface normal of the node. This is equivalent to a parallel shifting of the radius line to the tip of the shift vector δs. It is obvious from the drawing, that under these conditions, the particles center must perform the same shift as the node, so δs also describes the movement of the particles center.

The total movement of the right particle due to node shifting can be formulated as follows:

$$\delta \mathrm{P}r = \frac{\partial \mathrm{P}r}{\partial s_\perp}\delta s_\perp + \frac{\partial \mathrm{P}r}{\partial s_\parallel}\delta s_\parallel \tag{4.15a}$$

$$\delta \mathrm{P}\varphi = \frac{\partial \mathrm{P}\varphi}{\partial s_\perp}\delta s_\perp + \frac{\partial \mathrm{P}\varphi}{\partial s_\parallel}\delta s_\parallel \tag{4.15b}$$

$$\delta \mathrm{P}\omega = \frac{\partial \mathrm{P}\omega}{\partial s_\perp}\delta s_\perp + \frac{\partial \mathrm{P}\omega}{\partial s_\parallel}\delta s_\parallel \tag{4.15c}$$

The partial derivatives therein are obtained from the geometric relations in the above figures.

$$\frac{\partial \mathrm{P}r}{\partial s_\perp} = \lim_{\delta s_\perp \to 0} \frac{\mathrm{P}r' - \mathrm{P}r}{\delta s_\perp} \tag{4.16}$$

$$\frac{\partial \mathrm{P}\varphi}{\partial s_\perp} = \lim_{\delta s_\perp \to 0} \frac{\delta \mathrm{P}\varphi}{\delta s_\perp} \tag{4.17}$$

$$\frac{\partial \mathrm{P}r}{\partial s_\parallel} = \lim_{\delta s_\parallel \to 0} \frac{\mathrm{P}r' - \mathrm{P}r}{\delta s_\parallel} \tag{4.18}$$

$$\frac{\partial \mathrm{P}\varphi}{\partial s_\parallel} = \lim_{\delta s_\parallel \to 0} \frac{\delta \mathrm{P}\varphi}{\delta s_\parallel} \tag{4.19}$$

Of course, for each node the resulting movement of the particle will be different due to geometric relations and diffusive fluxes. The geometric relations are fixed for a regarded state, but the diffusive fluxes can be used to fulfill Equation 4.15 simultaneously for all nodes involved in a contact. So there is a set of equations available to describe particle contact conditions as constraints for the TEP-approach.

4.4 Considerations on Sinter Necks

4.5 Considerations on Grain-Matrix Interfaces

4.6 Application of the Thermodynamic Extremal Principle

In the following the generalized extremal principle is applied on the current model of particles and nodes, see subsubsection 1.2.5 for details on the approach. As before, an index of the currently regarded particle or node is neglected where appropriate for brevity. The indizes $\square_\mathrm{u}$ and $\square_\mathrm{l}$ are used to denote the upper resp. lower neighbor of a node. $\mathbb{N}$ is the set of all nodes present in the system and $\mathbb{P}$ the set of all particles, respectively.

4.6.1 Time Scale Definition

The application of the TEP results in ordinary differential equations in time which can be solved analytically for simple problems. Here, however, the problem is to complex to be solved analytically, so numerical time integration is required. Usually, the transition from infinitesimal description to finite time steps would be performed as a last step, but doing this step at the beginning opens possibilities of simplifying the equations and clarifies the following elaborations. At this point, it does not matter if a simple Eulerian integration is used or more complex methods like Runge-Kutta. The key feature is, that we use a finite time step width δt, which is fixed in each time step calculation, but may change from step to step. So, the internal state velocities $\dot{x}$ are directly linked linearly to finite changes using the time step as follows:

$$\delta x = \dot{x} \cdot \delta t \tag{4.20}$$

4.6.2 Choice of Variables

First, the internal state variables $\boldsymbol{x}$, the internal state velocities $\dot{\boldsymbol{x}}$ and the fluxes $\boldsymbol{j}$ must be chosen. The feasibility of the approach heavily depends on this choice.

The choice of the fluxes is straightforward with the diffusional fluxes. One has two diffusional fluxes on each node j_{u} and j_{l}, however the flux of the upper node to the lower and the flux from the lower to the upper are always equal due to constance of mass. Additional fluxes are to be found in the fluxes from the particle to the matrix Mj, if a matrix is present in the inter-particle spaces.

The internal state variables are the polar coordinates of the nodes $[r, \varphi]$ in with pole in their particle's center, since they determine the thermodynamic forces and the main aim of the simulation is to follow the time evolution of the particles and nodes. The coordinates of the particles $[\mathrm{P}r, \mathrm{P}\varphi, \mathrm{P}\omega]$ are not used as internal state variables, since they are unambiguously defined, if the coordinates of all nodes relative to their particle are known and also which nodes are in contact to each other. Moreover, the particle coordinates are auxiliary variables (included in $\boldsymbol{\xi}$) to ease formulation of the geometric constraints.

The straightforward choice of the internal state velocities are the finite changes of internal state variables (e.g. Δr and $\Delta \varphi$). However, for the changes in node coordinates this is not feasible, since they do not depend linearly on the fluxes due to triangular function relations. A more appropriate way is to define the node shifts $\delta s_{\perp}$ and $\delta s_{\parallel}$ as internal state velocities, so that the required constraints $\boldsymbol{f}$ become linear (see subsection 4.6.5). As they are determined, translation into new coordinates is directly possible using the relations obtained in the previous sections.

The external state variables (such as temperature T and pressure p) are not considered in the following, since they are assumed constant.

4.6.3 Dissipation $\mathcal{D}$

The dissipation at one node is given by the product node shifts and the respective Gibbs energy derivatives as in Equation 4.21. The Gibbs energy derivatives were determined in previous sections for the different node types. The dissipation of the whole system is the sum of all node dissipations, since all thermodynamic forces occur at nodes. Shifting of particles alone does not follow a thermodynamic force, but is determined by the ensemble of the involved nodes.

$$\mathcal{D} = \sum^{\mathbb{N}} \left[\frac{\partial G}{\partial s_{\perp}} \delta s_{\perp} + \frac{\partial G}{\partial s_{\parallel}} \delta s_{\parallel} \right] \tag{4.21}$$

4.6.4 Dissipation Function $\mathcal{Q}$

$$\mathcal{Q} = \sum^{\mathbb{N}} \frac{1}{2} \frac{RT}{V_\mathrm{m} \xi_\circ} \left(\frac{a_\mathrm{u} j_\mathrm{u}^2}{D_\mathrm{u}} + \frac{a_\mathrm{l} j_\mathrm{l}^2}{D_\mathrm{l}} \right) \delta t \tag{4.22}$$

4.6.5 Required Constraints $\boldsymbol{f}$

Relation between fluxes resp. volume change and shift.

$$\frac{\partial V}{\partial s_\perp} \delta s_\perp + \frac{\partial V}{\partial s_\parallel} \delta s_\parallel = \delta V = (j_\mathrm{u} + j_\mathrm{l})\, \delta t \tag{4.23}$$

4.6.6 Additonal Constraints $\boldsymbol{g}$

For each contact node, where:

$$\delta \mathrm{P}r = \frac{\partial \mathrm{P}r}{\partial s_\perp} \delta s_\perp + \frac{\partial \mathrm{P}r}{\partial s_\parallel} \delta s_\parallel \tag{4.24a}$$

$$\delta \mathrm{P}\varphi = \frac{\partial \mathrm{P}\varphi}{\partial s_\perp} \delta s_\perp + \frac{\partial \mathrm{P}\varphi}{\partial s_\parallel} \delta s_\parallel \tag{4.24b}$$

$$\delta \mathrm{P}\omega = \frac{\partial \mathrm{P}\omega}{\partial s_\perp} \delta s_\perp + \frac{\partial \mathrm{P}\omega}{\partial s_\parallel} \delta s_\parallel \tag{4.24c}$$

5 Software Implementation of the Model

Reference to open source code

5.1 Representation of Particles and Nodes

- Classes
- Tree Structure
- Coordinate Systems

5.2 Numerical Solution Procedure

- TEP Solution
- Time Step
- Monte-Carlo Drawing

5.3 Calculation and Extraction of Key Features

- Volume Cell, Shrinkage
- Neck Measures

6 Model Validation

6.1 Investigations on Simple Test Cases

6.1.1 A Single Particle Free in Space

6.1.2 A Particle Pair Free in Space

6.1.3 A Particle Pair at Different Contact Angles

6.1.4 A Particle Pair with Asymmetric Material Properties

6.1.5 A Single Particle Embedded in a Matrix

6.1.6 A Particle Pair Embedded in a Matrix

6.2 Experimental Validation Counter Bulk Sintering Trials

7 Summary and Outlook

List of Figures

4.1 Position of a Particle and Its Local Coordinate System 12
4.2 Contact of Two Particles with Respective Properties 13
4.3 Undirected Particle Graph Representing Contact Conditions 14
4.4 Directed Acyclic Graph Structure of Particle Contacts Rooted at Vertex 0 15
4.5 Ring Path Search Using a Depth-First Graph Search 16
4.6 Shifting of Surface Nodes 17
4.7 Change in Gibbs Energy Due to Node Shifting (tangents dashed) 18
4.8 Effect of Normal Node Shifting on Particle Postion 20
4.9 Effect of Tangential Node Shifting on Particle Postion 20

List of Tables

Bibliography

[1] F.D. Fischer, J. Svoboda, and H. Petryk. "Thermodynamic Extremal Principles for Irreversible Processes in Materials Science". In: *Acta Materialia* 67 (Apr. 2014), pp. 1–20. ISSN: 13596454. DOI: 10.1016/j.actamat.2013.11.050. URL: https://linkinghub.elsevier.com/retrieve/pii/S1359645413009087 (visited on 07/18/2023).

[2] Klaus Hackl, Franz Dieter Fischer, and Jiri Svoboda. "Constraints in Thermodynamic Extremal Principles for Non-Local Dissipative Processes". In: *Continuum Mechanics and Thermodynamics* 32.5 (Sept. 2020), pp. 1337–1345. ISSN: 0935-1175, 1432-0959. DOI: 10.1007/s00161-019-00846-3. URL: http://link.springer.com/10.1007/s00161-019-00846-3 (visited on 08/12/2022).

[3] Lars Onsager. "Reciprocal Relations in Irreversible Processes. I." In: *Physical Review* 37.4 (Feb. 15, 1931), pp. 405–426. ISSN: 0031-899X. DOI: 10.1103/PhysRev.37.405. URL: https://link.aps.org/doi/10.1103/PhysRev.37.405 (visited on 07/18/2023).

[4] J. Svoboda and I. Turek. "On Diffusion-Controlled Evolution of Closed Solid-State Thermodynamic Systems at Constant Temperature and Pressure". In: *Philosophical Magazine B* 64.6 (Dec. 1991), pp. 749–759. ISSN: 1364-2812, 1463-6417. DOI: 10.1080/13642819108207635. URL: https://www.tandfonline.com/doi/full/10.1080/13642819108207635 (visited on 08/11/2022).

[5] H. Ziegler. *An Introduction to Thermomechanics*. New York: North Holland Publishing, 1983.

[6] H. Ziegler. "Some Extremum Principles in Irreversible Thermodynamics, with Application to Continuum Mechanics". In: *Progress in Solid Mechanics* 4 (1963), p. 91.